

2022 年度 学位申請論文

**Treatment with hepatocyte transplantation
in a novel mouse model of persistent liver failure**

新規持続性肝不全マウスモデルにおける肝細胞移植治療

名古屋大学大学院医学系研究科
総合保健学専攻

(指導：石川 哲也 教授)

玉置 優貴

Treatment with hepatocyte transplantation in a novel mouse model of persistent liver failure

新規持続性肝不全マウスモデルにおける肝細胞移植治療

Yuki Tamaki

Course in Radiological and Medical Laboratory Sciences, Department of Integrated Health Sciences,

Academic adviser: Tetsuya Ishikawa

Abstract

Background and Aim: Cell-based transplantation therapy using hepatocytes, hepatic stem cells, hepatocyte-like cells induced from stem cells, etc. is thought to be an attractive alternative to liver transplantation, and have been studied to date. For its clinical application, however, it is extremely important to develop a model that reproduces the pathological conditions with indication for treatment and enables the study for the ideal treatment strategy.

Methods: The transgenic mice which express the thymidine kinase (TK) gene of human herpes simplex virus (HSV) in their hepatocytes with normal immunity has been developed (designated as HSVtk). After ganciclovir (GCV) administration which injure TK-expressing hepatocytes, the primary hepatocytes (PHs) isolated from green fluorescent protein (GFP) transgenic mouse (GFP-tg) were transplanted to HSVtk intrasplenically, and replacement index (RI) with transplanted PHs in the liver, liver histology, and mRNA expressions in the liver were analyzed up to 8 weeks after transplantation.

Results: HSVtk without PH transplantation after GCV administration developed persistent liver failure with degenerated hepatocytes, persistent elevation of ALT and hepatic p16 mRNA levels, suggesting the existence of cellular senescence in the base of the disease. When autologous GFP-PHs were transplanted to HSVtk, the transplanted cells were successfully engrafted in the liver. Eight weeks after transplantation, serum ALT levels and liver histology were almost normalized, while RIs varied from 19.8 to 73.8%. Since the hepatic p16 mRNA levels were decreased significantly in these mice, the senescence of hepatocytes associated with liver injury was thought to be resolved. On the other hand, allogenic GFP-PHs transplanted to HSVtk were eliminated as early as 1 week after transplantation. In these mice, hepatic p16 mRNA levels were significantly increased at 8 weeks after transplantation, suggesting the aggravation of hepatocyte senescence. FK506 administration to HSVtk protected the transplanted hepatocytes with allogenic background from rejection at 2 weeks after transplantation, but the condition of mice and the senescent status in the liver seemed worsened.

Conclusions: The mouse model with HSVtk/GCV system was useful for studying the mechanism of liver regeneration and the immune rejection responses in the hepatocyte transplantation treatment. It may also be utilized to develop the effective remedies to avoid immune rejection.

新規持続性肝不全マウスモデルにおける肝細胞移植治療

医学系研究科 総合保健学専攻 医療技術学コース

玉置 優貴

指導教員 石川 哲也

背景および目的：肝細胞や、肝幹細胞、幹細胞から誘導された肝細胞様細胞などは肝移植の代替となる有力な治療法であると考えられており、これまでに研究が進められてきた。しかし、その臨床応用のためには、治療の適応となる病態を再現し、治療戦略を検討できる理想的なモデルを開発することが非常に重要である。

方法：ヒト単純ヘルペスウイルス (HSV) のチミジンキナーゼ (TK) 遺伝子を肝細胞に発現し、正常な免疫能を有するトランスジェニックマウス (HSVtk とする) を作製した。TK 発現肝細胞を損傷させるはガンシクロビル (GCV) を投与後、緑色蛍光タンパク質 (GFP) 発現トランスジェニックマウス (GFP-tg) から分離された初代肝細胞 (PH) を HSVtk に脾臓内移植した。移植された PH による肝臓内の置換指数 (RI)、肝臓の組織学、および肝臓の mRNA 発現を、移植後 8 週間まで分析した。

結果：GCV 投与後、PH 移植なしの HSVtk (*Sham*) では、肝細胞の変性、ALT レベルや p16 の肝内 mRNA レベルの持続的な上昇を伴う持続性肝不全を発症し、疾患の根底に細胞老化が存在することが示唆された。同種同系の GFP-PHs を HSVtk に移植 (*Auto*) すると、移植細胞が肝臓内へ生着することが分かった。移植の 8 週間後、血清 ALT レベルと肝臓組織学はほぼ正常化されたが、RI は 19.8 から 73.8%まで変化を示した。*Auto* モデルでは、p16 の肝内 mRNA レベルが大幅に低下したため、肝障害に関連する肝細胞の老化が解消されたと考えられる。一方で、HSVtk に移植された同種異系の GFP-PH は、移植後 1 週間以内という短期間で排除された。これらのマウスでは、p16 の肝内 mRNA レベルが移植後 8 週間で有意に増加し、肝細胞老化の悪化が示唆された。また、FK506 を HSVtk に投与すると、移植後 2 週間で同種異系肝細胞が免疫拒絶反応から保護されたが、マウスの状態および肝臓の老化状態は悪化を示した。

結論：HSVtk/GCV システムを持つマウスモデルは、肝細胞移植治療における肝再生のメカニズムと免疫拒絶反応の研究に有用であった。また、免疫拒絶反応を回避するための効果的な治療法を開発するために利用することもできる。

Contents

Introduction	1
Materials and Methods	2-5
1. Animals.....	2
2. Primary hepatocyte (PH) isolation.....	2
3. Ganciclovir administration and PHs transplantation.....	2, 3
4. Treatment with tacrolimus against immune rejection of transplanted PHs	3
5. Preparation of Adipose-derived stem cells (ASC) and treatment against immune rejection with ASC .	3
6. Body weight measurement and sample collection after transplantation	3, 4
7. Histological analysis	4
8. Flow cytometry for DNA polyploidy analysis.....	4
9. Quantitative real-time reverse-transcription PCR (qRT-PCR) analysis.....	4, 5
10. Statistical analyses	5
Result	6-8
1. Sequential changes of BW and ALT levels.....	6
2. Replacement indices (RIs) by transplanted hepatocytes	6
3. Changes of liver histology.....	6, 7
4. Changes of nuclear sizes of the hepatocytes	7
5. The hepatic mRNA expression of cytokines/chemokines and cell surface markers.....	7, 8
6. The hepatic mRNA expression of growth factors and cell cycle-related molecules.....	8, 9
7. The hepatic mRNA expression of fibrosis markers	9
8. Therapeutic effect of FK506 or ASCs against immune rejection of transplanted hepatocytes	9, 10
Discussion	11-13
Acknowledgement	13
References	14-16

Figure legends	17, 18
Figures	19-23
Figure legends for supplementary figure	24
Supplementary figures	25-27
Supplementary tables	28-29

Introduction

Orthotopic liver transplantation (OLT) for intractable liver diseases, such as acute and chronic liver failure and hepatocellular carcinoma, is an effective remedy proven to improve prognosis of the patients [1,2]. But there are some serious problems in conducting liver transplantation, such as lack of donors, operative damages for both recipients and donors, risk of graft rejection, and side effects of immunosuppressants [3-6]. As a substitute for OLT, treatment based on cell transplantation, such as with hepatocytes, hepatic stem cells, and hepatocyte-like cells induced from somatic stem cells or iPS cells [7-10], and organoid transplantation [11], have been studied.

For the treatment of liver failure, the strategy to use mature hepatocytes for transplantation has been considered, and the clinical trials to prove its efficacy has continued for more than 2 decades [7]. Although its safety and short-term efficacy have been proven, there are unsolved issues, such as low cell engraftment rate and short-lasting effect. To solve such problems and guarantee the possibility of next-generation cell-based or organoid transplantation, the establishment of an appropriate model useful for studying an ideal methodology of cell-based transplantation therapy is extremely important.

Recently, the systems to develop human hepatocyte chimeric mice were established. The chimeric mice produced by these systems have been used mainly to reproduce hepatitis virus infection, such as hepatitis B and C virus (HBV and HCV) that infect human hepatocytes exclusively and test the effects of the antiviral drugs for these viruses. Furthermore, they have also been used to examine the metabolic efficiency of drugs and toxic substances which are known to be metabolized in human hepatocytes.

TK-NOG: severely immunodeficient NOG (NOD/SCID/IL2Rg null) mouse with targeted expression of the herpes simplex virus (HSV) type 1 thymidine kinase (TK) in the hepatocytes, has been used for developing the human hepatocyte chimeric mice. In TK-NOG mouse, the administration of ganciclovir (GCV) and subsequent transplantation of healthy human hepatocytes enables mouse liver to be stably replaced with mature and functional human hepatocytes [12,13]. Indeed, the hepatocyte chimeric mice developed from TK-NOG mice are recognized as very useful *in vivo* model for screening and assessment of the antiviral drugs for HBV and HCV [14]. However, at the same time, these mice have essential problem that they cannot reproduce the pathology of immunity-based liver damage, such as viral hepatitis because of their severe immunodeficiency.

In the current study, we modified TK-NOG mouse to have normal immunity in order to develop an appropriate model for hepatocyte or hepatocyte-like cell transplantation, with which the study for the mechanism of engraftment and immune rejection of the transplanted cells is possible. Namely, we backcrossed TK-NOG mice to BALB/c or C57BL/6 background, and designated these immunocompetent mice with TK expression in their hepatocytes as HSVtk mice. These HSVtk mice were transplanted with autologous or allogeneic hepatocytes after being administered with GCV. Then the mice were served for the sequential analysis of replacement rate with transplanted hepatocytes and histological and immunological changes in the liver caused by the transplantation. In addition, we examined the efficiency of immunosuppressive therapies with tacrolimus (FK506) [15-17] and adipose tissue-derived mesenchymal stem cells (ASCs) [18,19] to avoid immune rejection of the transplanted cells.

Materials and Methods

1. *Animals*

HSVtk mice expressing TK in the liver under the control of an albumin promoter, backcrossed onto inbred C57BL/6 or Balb/c and acquired normal immune system, were obtained from Central Institute for Experimental Animals (CIEA, Kawasaki, Japan). Backcrossing to the individual strains of mice was continued 9 to 10 times in our facility to establish HSVtk with complete inbred background of C57BL/6 (H-2^b) and BALB/c (H-2^d), and these mice were designated as HSVtk/BL6 and HSVtk/Balb, respectively (Fig. 1a, Suppl. Table 1). Green fluorescent protein (GFP)-transgenic mice with C57BL/6 background (GFP-tg, H-2^b) which systemically express GFP under the control of a chicken beta-actin promoter and cytomegalovirus enhancer (CAG promoter), were purchased from RIKEN Bio Resource Research Center (Kanagawa, Japan). C57BL/6 and BALB/c mice were purchased from Chubu Kagaku Shizai Co., Ltd. (Aichi, Japan). All the mice were housed in a controlled environment (12 h light/dark cycles at 25 °C) with free access to water and chow (CE2; CLEA Japan, Tokyo, Japan; DietGel Recovery, Clear H₂O, Portland, ME). All conditions and handling of animals in this study were conducted in accordance with the National Institutes of Health guide for the care and use of Laboratory animals (NIH Publications No. 8023, revised 1978), and under the protocols approved by Nagoya University Committee on Animal Use and Care (#031-35, #20042, # D210671, #D220046). The numbers of mice used in the individual experiments are described in the figure legends.

2. *Primary hepatocyte (PH) isolation*

PHs were isolated from 6 to 11 weeks old GFP-tg. In brief, mice were anesthetized with isoflurane (Pfizer Inc., New York, NY), and the liver was rinsed with 20 ml prewarmed (47 °C) Liver Perfusion Medium (17703-038; Gibco) through the abdominal inferior vena cava. Then, the liver was perfused with Liver Digest Medium (17703-034; Gibco) containing LiberaseTM-TM (5401127001; Roche). The digested liver was aseptically transferred to a sterile tube containing 20 ml cold PBS. Isolated hepatocytes were dispersed into single cell suspension with a large bore pipette, and passed through a sterile 40 µm nylon mesh (Thermo Fisher Scientific Inc.) into a new sterile tube. The cell suspension passed through the mesh was centrifuged at 50×g at 4 °C for 3 min, and the resulting cell pellet was resuspended in cold PBS. Then the cells were counted, and viability of the cells were assessed using the trypan blue exclusion test.

3. *GCV administration and PHs transplantation*

GCV (Mitsubishi Tanabe Pharma Corp., Osaka, Japan) was intra- peritoneally administered to 7–10 weeks old HSVtk mice. For enabling engraftment of transplanted hepatocytes in the liver and avoiding loss of mice, it is necessary to adjust the ALT levels after GCV administration to 500–2000 U/L. Since HSVtk/Balb is more susceptible to GCV than HSVtk/BL6, the dose of GCV was adjusted to 50 µg/g (mouse weight) for HSVtk/Balb and 100 µg/g for HSVtk/BL6. One week after GCV administration, blood samples were subjected to the analysis of alanine aminotransferase (ALT) levels. ALT measurement was performed using transaminase CII-Test kit (Wako) or entrusted to SRL Inc. (Aichi, Japan). Transplantation was carried

out when ALT level reached 500 U/L or higher. In case ALT level was lower than 500 U/L, additional GCV administration was executed. One week after the last GCV administration, GCV-treated mice were transplanted with 1×10^6 of PHs (in 400 μ l PBS) from GFP-tg mice intrasplenically. HSVtk/BL6 and HSVtk/Balb transplanted with GFP-tg-derived PHs were defined as autologous PH transplantation (Auto) and allogenic PH transplantation model (Allo), respectively. HSVtk/BL6 without cell transplantation but injected with 400 μ l PBS alone was designated as Sham model (Fig. 1b, Suppl. Table 1).

4. Treatment with tacrolimus against immune rejection of transplanted PHs

FK506 stock (Astellas Pharmaceutical, Inc., Tokyo, Japan) was dissolved in PBS and adjusted to a working concentration of 0.08 mg/mL. For the treatment against immune rejection in *Allo* model, the mice were administered with 1.0mg/kg FK506 intraperitoneally every day from one day before transplantation [16, 17]. This model was designated as *FK* model (FK506-treated *Allo* model, Fig. 1c, Suppl. Table 1).

5. Preparation of Adipose-derived stem cells (ASC) and treatment against immune rejection with ASC

ASC were isolated as previously reported elsewhere with minor modification [18,19]. Inguinal subcutaneous adipose tissues were taken from 6 to 7 weeks old female BALB/c mice, the tissues were placed in Dulbecco's modified Eagle Medium Nutrient Mixture F-12 (DMEM, Life Technologies Corporation, NY, USA) containing 20% fetal bovine serum (FBS; Life Technologies), and minced finely adding 500 μ l of Hanks' balanced salt solution (HBSS; Life Technologies). The pooled, minced tissues were incubated in 10 ml of HBSS containing Collagenase Type I (Funakoshi Co Ltd, Tokyo, Japan) at 37 °C for 60 min. The suspensions of these tissues were passed through a sterile 100 μ m mesh, and resuspended in DMEM. After centrifugation at 1200 rpm for 10 min, the isolated cells were washed with DMEM and resuspended in DMEM containing 20%FBS. Then, the cells were seeded on 75 cm² flasks (Thermo Fisher Scientific Inc), the attached cells were cultured as the progenitors of ASCs. After 4 to 6 passages, thus cultured ASCs were used for the treatment against immune rejection of transplanted PHs. Namely, ASCs were collected, and 1×10^6 cells were resuspended in 190 μ l PBS with 10 μ l Novo-Heparin (1,000 Units/mL, Mochida Pharmaceutical, Tokyo, Japan), and administered via the tail vein on the day of PH transplantation and 3, 6 days after transplantation in *Allo* model [20]. This model was designated as *ASC* model (ASC-treated *Allo* model, Fig. 1c, Suppl. Table 1).

6. Body weight measurement and sample collection after transplantation

Body weight (BW) measurement and blood sample collection were performed at the time of GCV administration, and weekly after PH transplantation. Sera were stored at - 20°C until use, and they were subjected to the measurement of serum ALT levels (SRL Inc. Aichi, Japan). In all the models (*Sham*, *Auto*, *Allo*, *FK*, and *ASC* models), the mice were sacrificed at before (day 0) and 1 week after GCV administration (0 w), 1, 2, 4, and 8 to 11 weeks after PH transplantation (1, 2, 4, and 8 w, respectively). The resected livers were subjected to the histological analysis, flow cytometric analysis for hepatocyte polyploidy, and hepatic gene expression analysis (Fig. 1b and c). The part of liver tissues was fixed with 10 N Mildfolm (Wako) at

room temperature for the histological examination. The unfixed liver tissues were embedded with FSC 22 Clear Frozen Section Compound (Leica Biosystems, Germany), and frozen in liquid nitrogen for the preparation of frozen specimens also for another histological examination. The remaining part of them were stored at -30°C in RNAlater (QIAGEN, Hilden, Germany) for the analysis of mRNA expression. For the flow cytometric analysis, the livers were perfused as described above (2.2 PH isolation) to collect isolated hepatocytes.

7. *Histological analysis*

The fixed liver tissue was embedded with paraffin and sliced to a thickness of 4 µm by using a microtome. Staining with hematoxylin & eosin (HE), Azan, and immunostaining for GFP and Proliferating Cell Nuclear Antigen (PCNA) was performed using tissue specimens. The unfixed liver tissue was sliced to thickness of 8 µm by using a cryostat, and stained with senescence-associated β-galactosidase (SA-β-gal).

GFP and PCNA-immunostaining was performed according to the Cell Signaling Technology's protocol for immunochemical staining (paraffin). GFP (D5.1) XP® Rabbit mAb (Cell Signaling Technology, Danvers, MA) was diluted 200 times, and PCNA (D3H8P) XP® Rabbit mAb (CST) 4000 times for use. The Senescence β-Galactosidase Staining Kit (CST) was used according to manufacturer's instructions for β-gal staining.

The liver specimens were microscopically observed and photographed by DP 73 (analyzed by Cell sense, Olympus, Tokyo, Japan), and the overall images of the livers with immunostaining was taken with BZ-9000 (Keyence, Osaka, Japan). The percentages of GFP immunostaining-positive part (replacement index: RI) and the area of Azan staining-positive region were quantified using ImageJ (Wayne Rasband, NIH, USA). The images of HE- and PCNA-stained specimens were examined using BZ-X800 (Keyence) and BZ-X800 Analyzer software for the measurement of nucleus sizes and PCNA positive ratios.

8. *Flow cytometry for DNA polyploidy analysis*

Cell Cycle Phase Determination Kit (Cayman chemical company) was used to analyze cell cycle alterations and DNA polyploidy in PHs isolated from the *Allo* model at 8 w. The collected PHs were passed through a sterile 40 µm nylon mesh, and washed twice with cold PBS and assay buffer, respectively. After the centrifugation, the cell pellet was resuspended to density of 1 x 10⁶ cells/ ml in assay buffer, and added an equal volume of cell cycle phase determination fixative to each sample to fix and permeabilize the cells and place at -20°C for at least 2 h. The fixed cells were centrifuged at 500 G for 5 min, and resuspended in 0.5 ml staining solution. After incubating for 30 minutes at room temperature in the dark, the samples were analyzed using FACS Canto2 (BD Biosciences).

9. *Quantitative real-time reverse-transcription PCR (qRT-PCR) analysis*

Quantitative real-time reverse-transcription polymerase chain reaction (qRT-PCR) was performed using total RNA prepared from liver tissue with NucleoSpin® RNA (Takara Bio Inc., Shiga, Japan). The RNA was subjected for first-strand cDNA synthesis using PrimeScript RT Master Mix (Takara Bio Inc.) according to

the manufacturer's instructions. qRT-PCR was performed with Thermal Cycler Dice Real Time System II (Takara Bio Inc.) using TB Green™ Premix Ex Taq™ II (Tli RNaseH Plus, Takara Bio Inc.) according to the manufacturer's instructions. The PCR amplification was performed as follows; an initial denaturing step, at 95°C for 30 seconds; followed by 40 cycles, at 95°C for 5 seconds; at 60°C for 30 seconds. Measured items and their primers in this experiment are listed in Suppl. Table 2.

10. Statistical analyses

All the values were expressed as the mean \pm SD (standard deviations). Data were analyzed by two-way analysis of variance test (ANOVA) followed by Steel-Dwass tests for multiple group comparison. All analyses were performed with EZR (Saitama Medical Center, Jichi Medical University, Saitama, Japan) [21], which is a graphical user interface for R (The R Foundation for Statistical Computing, Vienna, Austria). A significant difference was defined as a p-value of <0.05 .

3. Results

1. Sequential changes of BW and ALT levels

First, we evaluated sequential changes of BW and serum ALT levels in *Sham*, *Auto*, and *Allo* models. BW ratios (the ratios of BW at the individual time point to BW just before PH transplantation) and serum ALT levels were weekly measured from 0 to 8 w. There were no significant changes in BW ratios and ALT levels among three models until 4 w. However, BW ratios were significantly higher and ALT levels were significantly lower in the *Auto* model compared with the *Sham* and *Allo* models at 8 w. ($p < 0.05$, respectively, Fig. 2a, b, Suppl. Table 3a, b). These indicate that the nutritional status and liver injury were ameliorated only in the *Auto* model.

2. Replacement indices (RIs) by transplanted hepatocytes

In the *Auto* model, GFP immunostaining indicated that average RIs by the transplanted GFP-expressing hepatocyte at 1, 2, 4, and 8 w were $1.2 \pm 1.5\%$, $11.5 \pm 13.2\%$, $28.1 \pm 6.1\%$ and $46.2 \pm 23.2\%$, respectively (Fig. 3b). RIs of 8 w varied from 19.8 to 73.8%. Representative image of the whole liver immuno-stained with GFP (that of HSVtk at 8 w showing RI of 54.7%) is presented in Suppl. Fig. 1a, and those of the GFP-stained liver sections at the individual time points are presented in Fig. 3a. These indicate that the transplanted, engrafted hepatocytes gradually proliferated at least up to 8 w in the *Auto* model. On the other hand, in the *Allo* model, the GFP-positive hepatocytes were not detected both in the histological and qRT-PCR analysis already at 1 w (Fig. 3b, c), indicating that the transplanted PHs were eliminated before one week after the transplantation or earlier.

3. Changes of liver histology

The histological images of HE staining in each model are shown in Fig. 4a. In all the models at 0 w, many of the hepatocytes were degenerated with enlarged eosinophilic cytoplasm, and sporadic infiltration of inflammatory cells were observed mainly in the lobules. Apoptosis-like cells scattered in the lobules were observed at 0 w. In the *Sham* and *Allo* models, the extent of hepatocyte degeneration worsened over time, and most of the hepatocytes were degenerated at 8 w. Furthermore, inflammatory cell infiltration was continuously observed up to 8 w, but apoptotic cells and necrotic foci were rarely observed in both models. In the *Auto* model, inflammatory cell infiltration tended to be pronounced compared with in the *Sham* and *Allo* models at 2 w, but it decreased at 4 w and almost disappeared at 8 w. The extent of degeneration in the hepatocytes were reduced at 4 w, and most of the hepatocytes exhibited a nearly normal morphology at 8 w.

In Azan staining, no apparent fibrosis was observed at any time point in the *Auto* model. On the other hand, slight fibrosis around hepatocytes was observed in the *Sham* model at 8 w, and they were more evident in the *Allo* model at 8w. The areas of Azan staining-positive regions quantified by the image analysis were significantly increased at 4 and 8 w compared with those at 2 w or earlier in the *Sham* and *Allo* models, and the increase was more evident in the *Allo* model than in the *Sham* model. Azan staining-positive regions was not observed in the *Auto* model. (Fig. 4b).

Interestingly, there were clusters of small hepatocytes resembling regenerating nodules adjacent to the portal region only in the *Sham* and *Allo* models at 8 w (Suppl. Fig. 1b). It is possible that these small hepatocytes forming the nodules were differentiated from the hepatic stem cells in the canals of Hering, and it suggests that current model well reproduced the features of severe persistent liver failure.

4. Changes of nuclear sizes of the hepatocytes

We evaluated the proliferation efficiency of the hepatocytes by examining the percentages of PCNA-positive nuclei during the observation period in all the models. The rates of PCNA-positive nuclei at 8 w showed no apparent changes among the individual models (Fig. 4c). Since the nuclear enlargement was histologically observed in the *Sham* and *Allo* models, the sizes of hepatocyte nuclei were quantized during the observation period to determine whether the percentage of PCNA-positive nuclei truly reflected the degree of cell proliferation.

The sizes of nuclei were evaluated using images of HE staining. In the *Auto* model they were slightly larger after transplantation compared with those before transplantation, but the changes were not prominent. In contrast, the sizes of nuclei in the *Sham* and *Allo* models increased over time during the observation period, and this tendency was more prominent in the *Allo* model. When nuclear sizes were plotted as histograms, their variance was greater in the *Sham* and *Allo* models compared with the *Auto* model. (Suppl. Fig. 2).

We performed quantitative analysis of DNA in cell nuclei by flow cytometry to confirm if the enlargement of nuclei was associated with polyploidy, but no polyploidy was observed in the hepatocytes in the *Allo* model at 8 w (data not shown). Therefore, the enlargement of the nuclei was thought to be related to impairment of DNA replication and subsequent impairment of nucleus/cell division.

5. The hepatic mRNA expression of cytokines/chemokines and cell surface markers

To elucidate the mechanism of liver regeneration and immune rejection against transplanted hepatocytes, we investigated hepatic mRNA expression related to inflammatory responses.

First, we analyzed the sequential changes of mRNA expressions of inflammatory cytokines. In the *Sham* model, the mRNA levels of TNF- α (*Tnfa*) and TGF- β (*Tgfb*) remained high until 8 w compared with those at day 0. The mRNA levels of IL-1 β (*Il1b*), IL-6 (*Il6*) and IL-10 (*Il10*) also showed same tendency while they tended to decline at 8 w.

In the *Auto* model, the mRNA levels of TNF- α , IL-1 β , IL-10, and TGF- β peaked at 1 to 2 w, declined thereafter, and fell to the levels equivalent to those of day 0 by 8 w. The mRNA levels of IL-6 also showed similar tendency. Notably, TNF- α and TGF- β mRNA levels at 2 w were significantly higher in the *Auto* model than in the *Sham* model ($p < 0.05$).

In the *Allo* model, the mRNA levels of all the cytokines increased at 0 w and remained elevated until 8 w. Particularly, the mRNA levels of TNF- α , IL-1 β , and IL-6 tended to increase at 8w (Fig. 6a).

Next, we analyzed mRNA expression of the cell surface makers of inflammatory cells. In the *Auto* model, the mRNA levels of CD3 (*Cd3*), CD8a (*Cd8a*), CD11b (*Cd11b*), CD11c (*Cd11c*), and NKp46

(*Nkp46*) peaked at 1 to 2 w, declined thereafter, and tended to fall to the levels at 0 w or lower by 8 w. The mRNA levels of CD8a, CD11b, CD11c in the *Auto* model were significantly higher than those in the *Sham* model at 1 or 2 w ($p < 0.05$), while the mRNA levels of CD11b and CD11c in the *Auto* model became lower than those in the *Sham* model at 8 w ($p < 0.05$). In the *Sham* and *Allo* model, the changing patterns in the mRNA levels of CD3, CD8a, CD11b, CD11c, and NKp46 showed same tendency, namely they were increased at 0 w and maintained higher levels compared to day 0 levels until 8 w (Fig. 5b). There were no apparent differences in the kinetics of CD4 mRNA (*Cd4*) levels among all the models, all showing gradual decrease from 1 to 8 w. The mRNA levels of CD19 (*Cd19*) did not show significant changes during observation period in all the groups of mice (data not shown).

We also examined the sequential changes of hepatic mRNA levels of chemokines. Most of the chemokines showed the similar tendency to those of cell surface markers within the individual groups (Suppl. Fig. 3a). The mRNA kinetics of cell surface markers and cytokines/chemokines seem to correspond to the histological findings of the individual groups (Fig. 4a).

6. The hepatic mRNA expression of growth factors and cell cycle-related molecules

Since the histology suggested impaired liver regeneration in the *Sham* and *Allo* models, we examined the mRNA expression levels of growth factors and cell cycle-related markers.

The mRNA levels of HGF (*Hgf*) in the *Sham* and *Auto* models elevated during 0 to 2 w compared with the day 0 levels, and tended to decline thereafter. But HGF mRNA levels in the *Sham* model at 8 w tended to be elevated and was significantly higher than those in the *Auto* model. HGF mRNA levels in the *Allo* model were tended to be elevated throughout the observation period compared with levels at day 0 (Fig. 5c). EGF (*Egf*), TGF- α (*Tgfa*), and VEGF (*Vegf*) mRNA levels were elevated compared with the day 0 levels in all the models from 0 to 8 w. In the *Auto* and *Allo* models, VEGF mRNA levels were highest at 8w during the observation period (Suppl. Fig. 3b).

HGF is known to be the most potent growth factor for hepatocytes, and its production is stimulated by inflammatory cytokines, such as IL-1, TNF- α , and IL-6. It is also known to be produced in hepatic stellate cells (HSCs) and liver sinusoidal endothelial cells (LSECs) [22]. The reason why the increase in HGF in the *Allo* model was not as high as in the *Sham* and *Auto* models is unknown, but it may be related to the influence on LSECs or HSCs by the rejection responses of the transplanted PHs.

The mRNA levels of p16 (*P16*) and p21 (*P21*) which are related to the cell-cycle regulation and also known as markers of cellular senescence, were evaluated.

In the *Sham* model, the mRNA levels of both p16 and p21 were increased at 0 w compared with those of day 0 levels. The mRNA levels of p16 remained high up to 4 w, and further increased at 8 w. On the other hand, the mRNA levels of p21 declined from 2 w, and became lower than those of day 0 after 4 w.

In the *Auto* model, the mRNA levels of p16 increased at 0 w, temporally decreased at 1w, increased again to the higher levels at 2, 4 w, and decreased to the 2 w levels at 8 w. The mRNA levels of p21 increased at 0 w, decreased at 1 and 2 w, and further decreased at 4 and 8 w below the levels at day 0.

The mRNA levels of p16 and p21 at 1 and 8 w in the *Auto* model were significantly lower than those in the *Sham* model ($p < 0.05$).

In the *Allo* model, the kinetics of p16 and p21 mRNA levels were similar to those of the *Sham* model. However, p16 and p21 mRNA levels at 1 and 2 w were significantly lower than those in the model without PH transplantation ($p < 0.05$).

While p16 and p21 are used as cellular senescence markers, p16 is considered to be a more favorable cellular senescence marker [23]. Although the β -gal staining of the liver specimen did not efficiently identify positive cells (data not shown), elevated p16 mRNA levels at 4 to 8 w in the *Sham* and *Allo* models were thought to associate with the senescence of hepatocytes in these models. And it appears to be consistent with the findings of histological features and impaired DNA replication in hepatocytes in these models.

The mRNA levels of Cyclin D (*Cyclin d*) and Cyclin E (*Cyclin e*) in all the models were also elevated compared with those of day 0 levels, while those in the *Auto* model tended to decline at 8 w (Suppl. Fig. 3b). These also suggests the existence of cell cycle arrest in G1/G2 phase in these models.

7. The hepatic mRNA expression of fibrosis markers

Liver fibrosis usually develops as a result of persistent inflammation in the liver. Without alleviation of inflammation, liver fibrosis eventually progresses and results in the development to liver cirrhosis. Since we observed fibrosis around hepatocytes in the *Sham* and *Allo* model at 4 to 8 w, we measured the mRNA levels of early profibrotic biomarker genes, procollagen type 1 (*Procollagen1*) and α -SMA (α -smooth muscle actin, *Sma*) to analyze the mechanism of liver fibrosis development, and Cytoglobin (*Cytoglobin*) mRNA levels as a biomarker of HSC activation.

In the *Auto* model, mRNA levels of all the markers increased until 2 w, but decreased thereafter to the level close to those of day 0. In the *Sham* and *Allo* models, mRNA levels of all the markers were increased compared to day 0 levels during the observation period, and it seems compatible to the emergence of fibrosis in the liver in these models (Fig. 5d).

Since we could not find apparent difference in mRNA levels of fibrosis markers between the *Sham* and *Allo* model, the reason why the extent of fibrosis was more severe in the *Allo* model than in the *Sham* model, could not be well explained.

8. Therapeutic effect of FK506 or ASCs against immune rejection of transplanted hepatocytes

Using the *Allo* model as an immune rejection model against transplanted hepatocytes, we tested the efficacy of FK506, potent inhibitor of T cell activation, and ASCs which show immunosuppressive effect on various inflammatory cells (Fig. 1c).

BW ratio of the *FK* model decreased compared with that of the *Allo* model at 2 w. ALT levels were not different between the *FK* and *Allo* model. On the other hand, in the *ASC* model, ALT levels mildly declined compared with those in the *Allo* model at 1 w, and the decrease of BW ratio was tended to be suppressed compared with the *Allo* model (Suppl. Fig.4a,b).

In the *FK* model, engraftment of GFP-positive hepatocytes was confirmed both in histology with GFP immunostaining and hepatic expression of GFP mRNA. However, HE staining showed degeneration of many of the hepatocytes and considerable inflammatory cell infiltration in the *FK* model as seen in the *Allo* model. In the *ASC* model, engraftment of GFP-positive hepatocytes was not observed, but the extent of hepatocyte degeneration and inflammatory cell infiltration seemed milder than in the *Allo* and *FK* models (Fig.6a, Suppl. Fig. 4d).

In order to analyze the mechanism of action of the treatment, we examined hepatic mRNA expression of cytokines, cell surface markers, etc. In the *FK* model, IFN- γ mRNA levels were significantly lower compared with those in the *Allo* and *ASC* models ($p < 0.05$), and CD3 and CD8a mRNA levels were significantly lower compared with those in the *Allo* model ($p < 0.05$). In the *ASC* model, IL-10 mRNA levels were significantly higher and CD11b significantly lower compared with those in the *FK* model ($p < 0.05$). The mRNA levels of p16 were significantly lower in the *ASC* model compared with those in the *Allo* model ($p < 0.05$), while p16 mRNA levels in the *FK* model showed tendency to be high compared with the other models (Fig.6b).

These results indicate that suppressing T-cell immunity is necessary to avoid rejection, but not sufficient for controlling inflammation, avoiding cellular senescence, and promoting liver regeneration. ASC therapy is thought to have the potential to modulate inflammation, but not to avoid rejection.

In order to avoid rejection and efficiently progress liver regeneration, it seems necessary to consider a combination of these treatments or to establish a new treatment strategy.

Discussion

In the current study, we have established HSVtk mice with normal immunity, and the liver regeneration model by transplanting of isolated hepatocytes into the HSVtk mice after GCV administration. Using this system, we investigated the process of hepatocyte engraftment and rejection after transplantation, and the sequential changes in liver histology and hepatic environment which relate to regeneration of the liver.

The combination of human TK and GCV is a system to cause death to target cell and often used for gene therapy of cancer [24,25]. GCV is selectively converted by TK to a guanosine analogue, into a monophosphorylated form which is then further phosphorylated. The generated GCV triphosphate causes chain termination by incorporation into replicating DNA as well as inhibition of DNA polymerase alpha, thereby causes apoptosis in the TK expressing cells. In addition, GCV-triphosphate is cytotoxic and causes cell death to the neighboring cells even without TK expression, and it may cause nonapoptotic cell death to those cells [26]. In the current study, we observed scattered apoptotic cells in the livers of the HSVtk mice at the early time point (0 w) after GCV administration. However, subsequent histological examination revealed that degenerated hepatocytes with enlarged cytoplasm and nuclei and inflammatory cell infiltration were the main histological findings, and apoptotic hepatocytes were rarely observed. These histological features, together with the increased mRNA levels of p16, p21, and those of inflammatory cytokines, such as TNF- α , IL-1 β , IL-6, and impairment of DNA replication, suggest the cellular senescence with cell cycle arrest in the hepatocytes is the main pathological condition in the HSVtk mice treated by GCV.

It has been recognized that cellular senescence and cell cycle arrest is involved in the pathogenesis of liver failure and various chronic liver diseases [27,28]. While the study for liver regeneration to date has been mainly executed using rodent models of partial hepatectomy [29,30], ischemia/reperfusion liver injury [31], and acute liver failure caused by CCl₄, concanavalin A. etc [32,33], we believe that the novel models used in the current study are more compatible for the study of liver regeneration treatment for the persistent or late-on-set liver failure.

In the *Auto* model, despite transplantation of rather small number of PHs of 1×10^6 , transplanted hepatocytes proliferated to nearly half of the hepatocytes in the liver (Fig. 3a-c). It is also notable that the resident hepatocytes recovered from the senescent condition, and the regained almost normal morphology with normal size and shape of nucleus and cytoplasm. It occurred even in the mice with low RIs.

In the *Auto* model, transient elevation of mRNA levels of inflammatory cytokines/chemokines, cell surface markers, and HGF at 1 and 2 w was characteristic compared to the other models, and its relation to the recovery of hepatocytes from senescent condition is likely. It has been reported that inflammatory cytokines and growth factors known to be induced during severe liver injury, such as TNF- α , IL-6, TGF- α , HGF, and EGF, promote survival and proliferation of hepatocytes [34,35]. Therefore, it is possible that some of these factors including TNF- α have closely related to hepatocyte recovery from cellular senescence and subsequent proliferation including transplanted PHs.

The molecules such as TNF- α , IL-1 β , HGF, and some chemokines, of which mRNA expression levels were elevated at 1 and 2 w in the *Auto* model, are promoted by NF κ B activation. They are identical to the

group of molecules produced through activation of NF κ B in senescent cells, which is called senescence-associated secretory phenotype (SASP) [36]. It is reasonable to assume that the transient increase in the mRNA expression of these molecules cannot be explained by cellular senescence alone, but is triggered by PH transplantation. There are various possibilities for this hypothesis, including the activation of the NF κ B pathway by interactions between transplanted PHs and LSECs, HSCs, and Kupffer cells, or by the infiltrating inflammatory cells, such as T cells and macrophages, but they have not been elucidated in the current study.

Regarding the above hypothesis, one notable point is the transient decline in p21 mRNA levels at 1 and 2 w in the *Auto* and *Allo* models, both received PH transplantation. Regarding this phenomenon, we considered the involvement of Notch signaling pathway. While p21 is induced by its upstream molecule, p53, murine double minute 2 (Mdm2), an E3 ubiquitin ligase, is reported to cause the degradation of p53, as a major molecule involved in the suppression of p53 activity [37]. And Mdm2 is activated by Notch signaling and is reported to ubiquitinate and activate the intracellular portion of the Notch receptor [38]. It is also known that Notch signaling is involved in the activation of the NF κ B pathway [39].

However, given that p16 also showed a downward trend at the same time, other factors may also be considered. Since we do not have direct evidence for above hypothesis, further study is necessary to confirm it.

In the current study, we also tried to find the way to rescue transplanted allogenic PHs from the rejection by recipient immune system. Since liver fibrosis was enhanced in the *Allo* model compared with the *Sham* model, it is quite important to avoid the immune rejection in cell transplantation therapy to evade from this worrying outcome.

We tested the efficacy of FK506 and ASCs for the treatment against immune rejection, and found out that only FK506 enabled the engraftment of transplanted allogenic PHs. Therefore, the use of FK506 seems reasonable for the treatment against immune rejection. But there are some concerns about this treatment, such as loss of BW in the *FK* mice which made the continuation of the treatment difficult in the current study, and the tendency of increase in hepatic p16 and p21 levels which relates cellular senescence.

On the other hand, treatment with ASC did not prevent rejection, but did reduce inflammation and improved the condition of mice, including increase of BW. Furthermore, ASC administration also caused tendency to decrease the mRNA levels of p16 and p21, and possible improvement in histology. Mesenchymal stem cells including ASC are known to have regulatory effects on various inflammatory cells (probably other than CD8⁺ T cell) [18,19], and actually exerted an anti-inflammatory effect in this model as well. Therefore, it is thought that the immunoregulatory action of ASC may have suppressed the senescence of hepatocytes in this model. The usefulness of ASC administration itself for the treatment of liver failure should also be investigated.

There are several limitations and remained questions in the current study besides described above. Since the difference in the background of mice alter the sensitivity to GCV, comparison in hepatic histology and mRNA expressions between the *Sham* and *Allo* model should be more deliberately. We tried to adjust the ALT levels before transplantation in all the models, but we should have added the appropriate control for the

Allo model, such as HSVtk/Balb with GCV treatment. We did not have method to predict RI after hepatocyte transplantation, and had to sacrifice mice at each time point. If we have surrogate marker for RI, it may make the sequential analysis easier and long-term analysis possible. We may have to think about more extended method for gene expression analysis, such as RNA sequence and single-cell analysis, since there are many other genes of interest other than we analyzed in the current study, and the cells that constitute the liver are diverse. All of these should be considered in the further study.

In conclusion, the current HSVtk/GCV system was confirmed to be useful for studying the mechanism of liver regeneration and immune rejection responses in the hepatocyte and hepatocyte-like cell transplantation treatment, and for studying the effective treatment methods to avoid immune rejection.

Acknowledgement

The authors thank Ms. Machi Yamamoto, Kanako Yamazaki, Ai Imaida, Junko Hori, Mr. Ayumu Kanbe for technical assistance. This research is partially supported by JSPS KAKENHI Grant Number JP16K09354, JP21K07959, the program on the Innovative Development and the Application of New Drugs for Hepatitis B from Japan Agency for Medical Research and Development (AMED, #20fk0310106h0004, #21fk0310106s0605, #22fk0310516s0201).

References

- [1] Neuberger J. An update on liver transplantation: A critical review. *J Autoimmun.* 2016; 66: 51–9.
- [2] Soyama A, Eguchi S, Egawa H. Liver transplantation in Japan. *Liver Transpl.* 2016; 22: 1401–7.
- [3] Tasdogan BE, Akosman S, Gurakar M, Simsek C, Gurakar A. Update on liver transplantation: What is new recently? *Euroasian J Hepatogastroenterol.* 2019; 9: 34-39. doi: 10.5005/jp-journals-10018-1293.
- [4] Brown SB. Pros and cons of living donor liver transplant. *Gastroenterol Hepatol (NY).* 2008; 4: 622–4.
- [5] Itri JN, Heller MT, Tublin ME. Hepatic transplantation: postoperative complications. *Abdom Imaging.* 2013; 38: 1300–33.
- [6] López MM, Valenzuela JE, Alvarez FC, López-Alvarez MR, Cecilia CS, Paricio PP. Long-term problems related to immunosuppression. *Transpl Immunol.* 2006; 17: 31–5.
- [7] Iansante V, Mitry RR, Filippi C, Fitzpatrick E, Dhawan A. Human hepatocyte transplantation for liver disease: current status and future perspectives. *Pediatr Res.* 2018; 83: 232-240. doi: 10.1038/pr.2017.284.
- [8] LGhanem LY, Mansour IM, Abulata N, Akl MM, Demerdash ZA, El Baz HG, Mahmoud SS, Mohamed SH, Mahmoud FS, Hassan ASM. Liver macrophage depletion ameliorates the effect of mesenchymal stem cell transplantation in a murine model of injured liver. *Sci Rep* 2019; 9: 35. doi: 10.1038/s41598-018-37184-4.
- [9] Katsuda T, Matsuzaki J, Yamaguchi T, Yamada Y, Prieto-Vila M, Hosaka K, Takeuchi A, Saito Y, Ochiya T. Generation of human hepatic progenitor cells with regenerative and metabolic capacities from primary hepatocytes. *eLife.* 2019; 8: e47313. doi: 10.7554/eLife.47313.
- [10] Takayama K, Akita N, Mimura N, Akahira R, Taniguchi Y, Ikeda M, Sakurai F, Ohara O, Morio T, Sekiguchi K, Mizuguchi H. Generation of safe and therapeutically effective human induced pluripotent stem cell-derived hepatocyte-like cells for regenerative medicine. *Hepatol Commun.* 2017; 1: 1058-69.
- [11] Reza HA, Okabe R, Takebe T. Organoid transplant approaches for the liver. *Transpl Int.* 2021; 34: 2031-2045. doi: 10.1111/tri.14128.
- [12] Hasegawa M, Kawai K, Mitsui T, Taniguchi K, Monnai M, Wakui M, Ito M, Suematsu M, Peltz G, Nakamura M, Suemizu H. The reconstituted “humanized liver” in TK-NOG mice is mature and functional. *Biochem Biophys Res Commun.* 2011; 405: 405–10.
- [13] Yamazaki H, Suemizu H, Shimizu M, Igaya S, Shibata N, Nakamura M, Chowdhury G, Guengerich FP. In vivo formation of dihydroxylated and glutathione conjugate metabolites derived from thalidomide and 5-hydroxythalidomide in humanized TK-NOG mice. *Chem Res Toxicol.* 2012; 25: 274–6.
- [14] Kosaka K, Hiraga N, Imamura M, Yoshimi S, Murakami E, Nakahara T, Honda Y, Ono A, Kawaoka K, Tsuge M, Abe H, Hayes CN, Miki D, Aikata H, Ochi H, Ishida Y, Tateno C, Yoshizato K, Sasaki T, Chayama K. A novel TK-NOG based humanized mouse model for the study of HBV and HCV infections. *Biochem Biophys Res Commun.* 2013; 441: 230–5.
- [15] Fung JJ, Todo S, Jain A, Mccauley J, Alessiani M, Scotti C, Starzl TE. Conversion from cyclosporine to FK506 in liver allograft recipients with cyclosporine-related complications. *Transplant Proc.* 1990; 22: 6–12.
- [16] Yu Z, Zhou X, Yu S, Xie H, Zheng S. IL-15 is decreased upon CsA and FK506 treatment of acute rejection following heart transplantation in mice, *Mol Med Rep.* 2015; 11: 37–42.
- [17] Shao K, Lu Y, Wang J, Chen X, Zhang Z, Wang X, Wang X, Yang H, Liu G. Different effects of tacrolimus on innate and adaptive immune cells in the allograft transplantation, *Scand J Immunol.* 2016; 83: 119–27.

- [18] Nagaya R, Mizuno-Kamiya M, Takayama E, Kawaki H, Onoe I, Tanabe T, Nagahara K, Kondoh N. Mechanisms of the immunosuppressive effects of mouse adipose tissue-derived mesenchymal stromal cells on mouse alloreactively stimulated spleen cells, *Exp Ther Med*. 2013; 7: 17–22.
- [19] Lee DK, Song SU. Immunomodulatory mechanisms of mesenchymal stem cells and their therapeutic applications. *Cell Immunol*. 2018; 326: 68–76.
- [20] Shi M, Liu Z, Wang Y, Xu R, Sun Y, Zhang M, Yu X, Wang H, Meng L, Su H, Jin L, Wang FS. A pilot study of mesenchymal stem cell therapy for acute liver allograft rejection. *Stem Cells Transl Med*. 2017; 6: 2053–61.
- [21] Kanda Y. Investigation of the freely available easy-to-use software ‘EZR’ for medical statistics. *Bone Marrow Transplant*. 2013; 48: 452-8. doi: 10.1038/bmt.2012.244.
- [22] DeLeve LD. Liver sinusoidal endothelial cells and liver regeneration. *J Clin Invest*. 2013; 123: 1861-1866. doi.org/10.1172/JCI66025.
- [23] Hara E, Smith, ParrybRD, Tahara H, Stone S, Peters G. Regulation of p16^{CDKN2} expression and its implications for cell immortalization and senescence. *Mol Cell Biol*. 1996; 16: 859-67. doi: 10.1128/MCB.16.3.859.
- [24] Mesnil M, Yamasaki H. Bystander effect in herpes simplex virus-thymidine kinase/ganciclovir cancer gene therapy: role of gap-junctional intercellular communication. *Cancer Res*. 2000; 60: 3989-99.
- [25] Al-Hendy A, Magliocco AM, Al-Tweigeri T, Braileanu G, Crellin N, Li H, Strong T, Curiel D, Chedrese PJ. Ovarian cancer gene therapy: repeated treatment with thymidine kinase in an adenovirus vector and ganciclovir improves survival in a novel immunocompetent murine model. *Am J Obstet Gynecol*. 2000; 182: 553-9. doi: 10.1067/mob.2000.104837.
- [26] Srivastava D, Joshi G, Somasundaram K, Mulherkar R. Mode of cell death associated with adenovirus-mediated suicide gene therapy in HNSCC tumor model. *Anticancer Res*. 2011; 31: 3851-7.
- [27] Mitselou A, Karapiperides D, Nesseris I, Vougiouklakis T, Agnantis NJ. Altered expression of cell cycle and apoptotic proteins in human liver pathologies. *Anticancer Res*. 2010; 30: 4493-501.
- [28] Huda N, Liu G, Hong H, Yan S, Khambu B, Yin XM. Hepatic senescence, the good and the bad. *World J Gastroenterol*. 2019; 25: 5069-5081. doi: 10.3748/wjg.v25.i34.5069.
- [29] Togo S, Makino H, Kobayashi T, Morita M, Shimizu T, Kubota T, Ichikawa Y, Ishikawa T, Okazaki Y, Hayashizaki Y, Shimada H. Mechanism of liver regeneration after partial hepatectomy using mouse cDNA microarray. *J Hepatol*. 2004; 40: 464-71. doi: 10.1016/j.jhep.2003.11.005.
- [30] Itoh T, Miyajima A. Liver regeneration by stem/progenitor cells. *Hepatology*. 2014; 59: 1617-26. doi: 10.1002/hep.26753. Epub 2014 Feb 14.
- [31] Konishi T, Lentsch AB. Hepatic ischemia/reperfusion: mechanisms of tissue injury, repair, and regeneration. *Gene Expr*. 2017; 17: 277-87. doi: 10.3727/105221617X15042750874156.
- [32] Meng Z, Wang Y, Wang L, Jin W, Liu N, Pan H, Liu L, Wagman L, Forman BM, Huang W. FXR regulates liver repair after CCl₄-induced toxic injury. *Mol Endocrinol*. 2010; 24: 886-97. doi: 10.1210/me.2009-0286.
- [33] Ya'acov AB, Meir H, Zolotaryova L, Ilan Y, Shteyer E. Impaired liver regeneration is associated with reduced cyclin B1 in natural killer T cell-deficient mice. *BMC Gastroenterol*. 2017; 17: 44. doi: 10.1186/s12876-017-0600-2.
- [34] Zimmers TA, McKillop IH, Pierce RH, Yoo JY, Koniaris LG. Massive liver growth in mice induced by systemic interleukin 6 administration. *Hepatology*. 2003; 38: 326–34.
- [35] Böhm F, Köhler UA, Speicher T, Werner S. Regulation of liver regeneration by growth factors and cytokines. *EMBO*

Mol Med. 2010; 2: 294-305. doi: 10.1002/emmm.201000085.

[36] Salama R, Sadaie M, Hoare M, Narita M. Cellular senescence and its effector programs. *Genes Dev.* 2014; 28: 99-114. doi: 10.1101/gad.235184.113.

[37] Vermeulen K, Berneman ZN, Van Bockstaele DR. Cell cycle and apoptosis. *Cell Prolif.* 2003; 36:165-75. doi: 10.1046/j.1365-2184.2003.00267.x.

[38] Dutta D, Sharma V, Mutsuddi M, Mukherjee A. Regulation of Notch signaling by E3 ubiquitin ligases. *FEBS J.* 2022; 289: 937-954. doi: 10.1111/febs.15792.

[39] Ayaz F, Osborne BA. Non-canonical notch signaling in cancer and immunity. *Front Oncol.* 2014; 4: 345. doi: 10.3389/fonc.2014.00345.

Figure legends

Fig. 1. Experimental scheme.

- a. The construction of HSVtk model. TK-NOG mouse is a transgenic mouse with NOG background, in which the mouse albumin enhancer/promoter (mAlb E/P), the chimeric intron, HSVtk cDNA, and the 3'-UTR of the human growth hormone gene with a polyadenylation signal (hGH pA) are integrated in its genome, and expresses HSV-TK only in the liver. We established an immunocompetent mice by backcrossing TK-NOG mice to C57BL/6 or BALB/c mice 9-10 times or more (designated as HSVtk/BL6 and HSVtk/Balb).
- b. Method of hepatocytes transplantation. GCV was intraperitoneally injected to HSVtk/BL6 or HSVtk/Balb, and primary hepatocytes (PHs) isolated from GFP-tg were transplanted after the ALT level reached 500 U/L (*Auto* or *Allo* model). HSVtk/BL6 administered with PBS after administered of GCV was used a control (*Sham*).
- c. Treatment model for immune rejection against allogenic hepatocytes. HSVtk/Balb after GCV administration was transplanted with PHs isolated from GFP-tg with BL/6 background (*Allo* model). FK506 was intraperitoneally administered every day from the day before transplantation until the day of sacrifice (*FK-treated* model). ASCs were intravenously administered three times on the day of transplantation, 3 days and 6 days after transplantation (*ASC-treated* model). *Allo* model without treatment was used as control. All the mice were sacrificed for analyses two weeks after transplantation.

Fig. 2. Changes of BW and ALT levels.

- a. Sequential changes of BW ratios in *Sham*, *Auto*, *Allo* models. The BW ratio (the ratio of BW at each time point to BW just before PH transplantation) was calculated for each week until 8 weeks after PH transplantation. 0 w means the time point before PH transplantation. All the data are expressed as mean \pm SD. * $p < 0.05$ (*Auto* vs *Sham* on same week), † $p < 0.05$ (*Allo* vs *Auto* on same week). $n = 3$ in each group.
- b. Sequential changes of ALT levels in *Sham*, *Auto*, *Allo* models. ALT levels were measured every week from 0 to 8 weeks after PH transplantation. All the data are expressed as mean \pm SD. * $p < 0.05$ (*Auto* vs *Sham* on same week), † $p < 0.05$ (*Allo* vs *Auto* on same week). $n = 3$ in each group.

Fig. 3. Engraftment of transplanted PHs.

- a. GFP-immunostaining in the liver of *Auto* model. Representative histological images of GFP-immunostained liver sections from the mice sacrificed at each time point (time after PH transplantation) are presented. From left to right, the liver images of the mice 1, 2, 4, 8 weeks after transplantation, respectively. $2 \times$ objective's scale bar: 200 μm , $20 \times$ objective's scale bar: 20 μm .
- b. Average values (%) of hepatocyte replacement indices (RIs). GFP-positive areas of the tissue samples were calculated using ImageJ. All the data are expressed as mean \pm SD. * $p < 0.05$. $n = 3$ in each group.
- c. Hepatic GFP mRNA expression in *Auto* and *Allo* models. Hepatic mRNA expression levels were

measured by qRT-PCR. Expression levels of the respective mRNAs were normalized to that of GAPDH and the data were presented as fold change compared with the average of *Auto* model at 1 week after PH transplantation. All the data are expressed as mean \pm SD. * $p < 0.05$ $n = 3$ in each group.

Fig. 4. Liver histology.

- a. Histological analysis with H&E staining at day 0, 0 w (upper row) and each time point after PH transplantation in *Sham* (second row), *Auto* (third row), and *Allo* (lower row) models. Arrowheads (\uparrow) indicate the apoptosis-like cells. Magnification of objective $\times 20$ (scale bar: 20 μm).
- b. Histological analysis stained with Azan at day0 (upper row), 0w(second row) and 8 weeks after transplantation in *Sham* (third row), *Auto* (fourth row), and *Allo* (lower row) models. 4 \times objective's scale bar: 200 μm , 20 \times objective's scale bar: 20 μm . The graph shows the Azan-positive area measured by the Image J software. * $p < 0.05$. $n = 3$ in each group.
- c. Histological analysis stained with PCNA at day0 (upper row), 0w(second row) and 8 weeks after transplantation in *Sham* (third row), *Auto* (fourth row), and *Allo* (lower row) models. 4 \times objective's scale bar: 200 μm , 20 \times objective's scale bar: 20 μm .

Fig. 5. Hepatic mRNA expressions.

Intrahepatic mRNA expression levels were measured by qRT-PCR. Expression levels of the respective mRNAs were normalized to that of GAPDH. The normalized data were presented as fold change compared with HSVtk/BL6 at day 0 for *Sham* and *Auto* models, and HSVtk/Balb at day 0 for *Allo* model (* $p < 0.05$, $\dagger p < 0.05$ in comparison of the values between *Sham* and *Auto* models at the same time point) . All the items were listed in the order of upper graph, that of *Sham*, *Auto* and *Allo* model. All the data are expressed as mean \pm SD. $n = 3\sim 5$ in each group.

- a-c. The mRNA expression of inflammatory cytokines(a), cell surface lineage makers (b), growth factors (c), fibrosis makers (d).

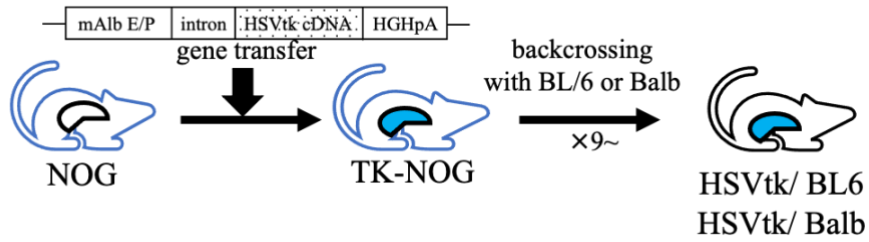
Fig. 6. The effect of the treatment against immune rejection.

- a. Liver histology in treatment models against immune rejection. H&E (upper row) and GFP immunostaining (lower row) of representative liver sections from each group of mice. From left to right, *Allo*, *FK-treated*, and *ASC-treated* models, respectively. Magnification of objective $\times 20$ (scale bar: 20 μm).
- b. Hepatic mRNA expressions in the treatment models. Hepatic mRNA expression levels were measured by qRT-PCR. Expression levels of the respective mRNAs were normalized to that of GAPDH, and presented as fold change compared with HSVtk/Balb day 0 for *Allo* model. All the data are expressed as mean \pm SD. * $p < 0.05$. $n = 3\sim 5$ in each group.

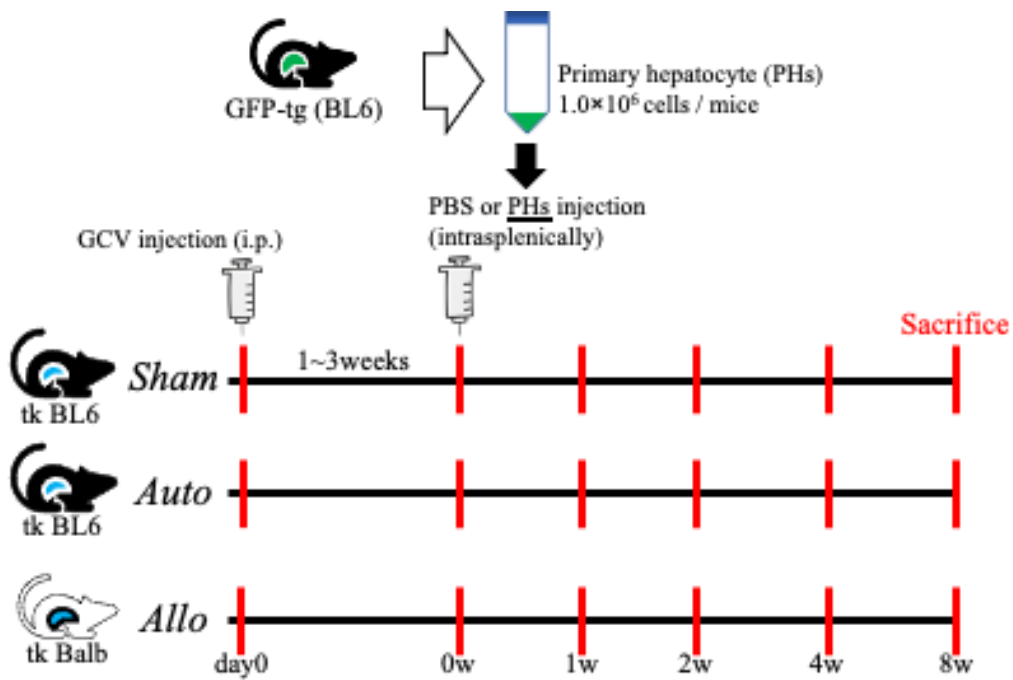
Figure1

(a)

TK model



(b)



(c)

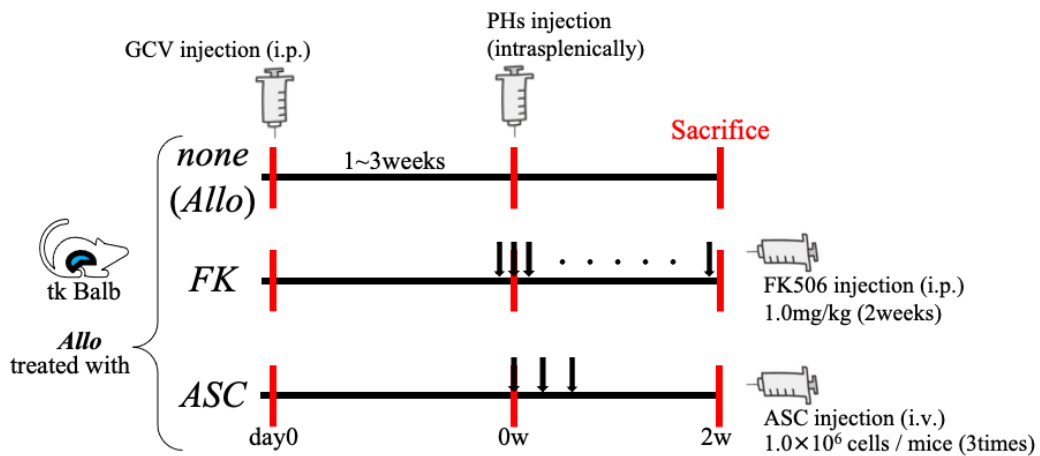


Figure2

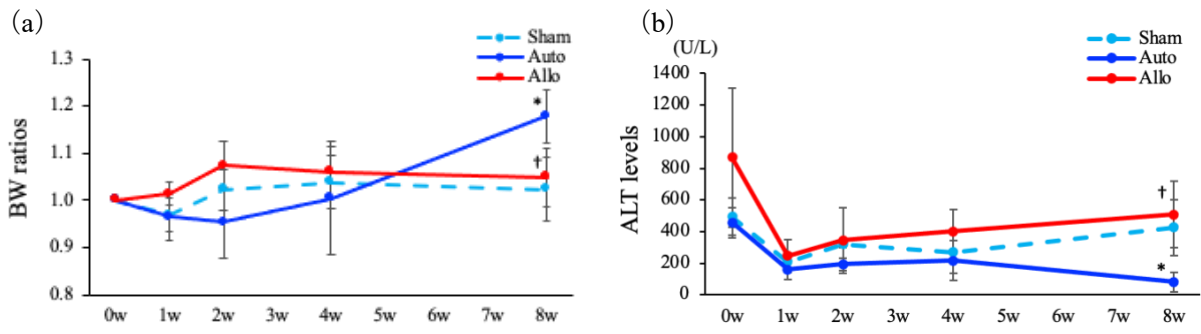


Figure3

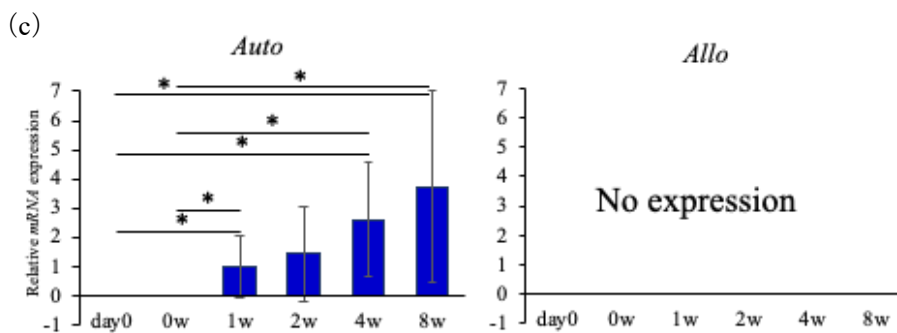
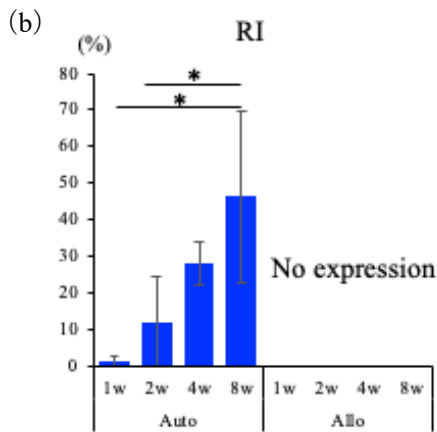
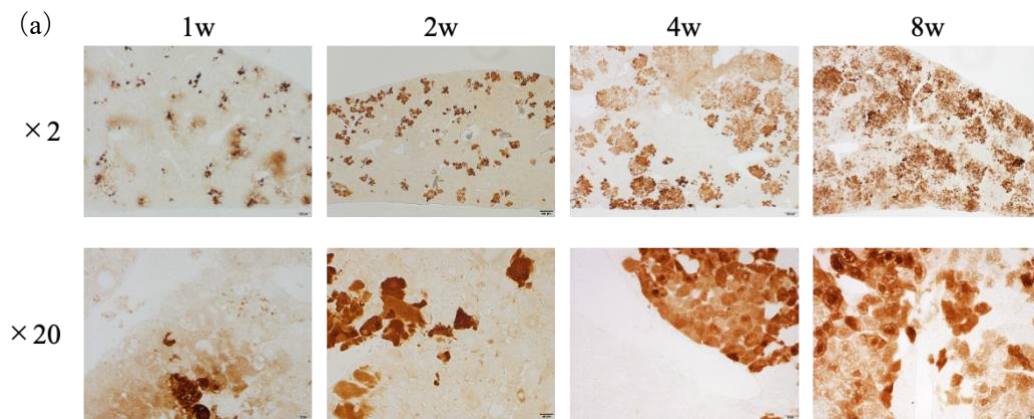
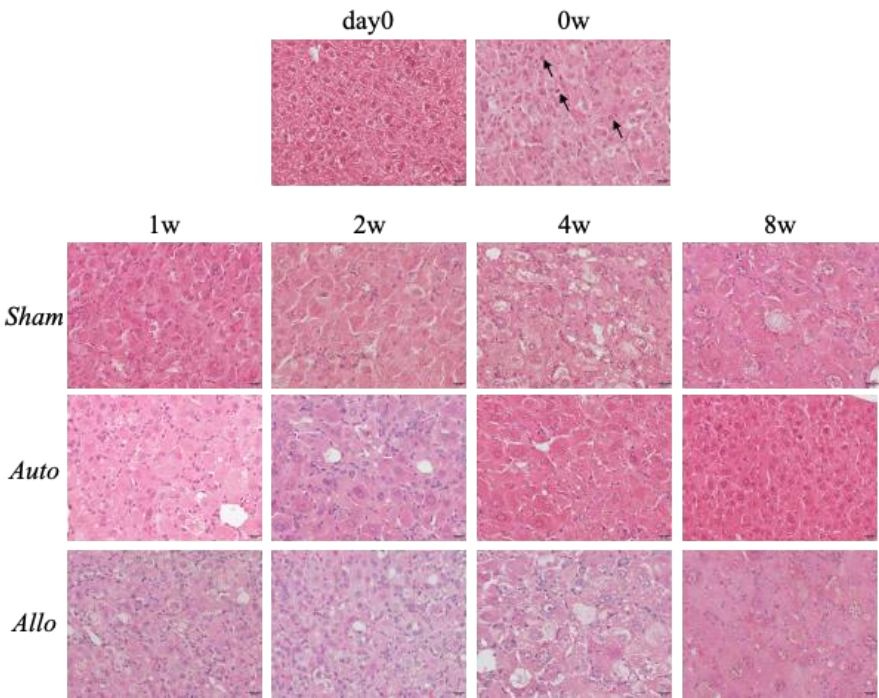
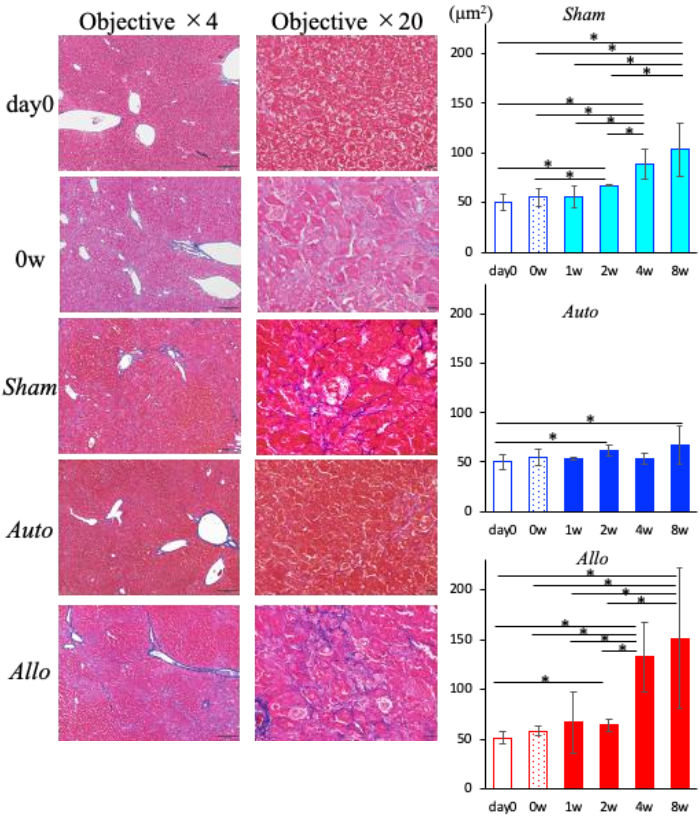


Figure4

(a)



(b)



(c)

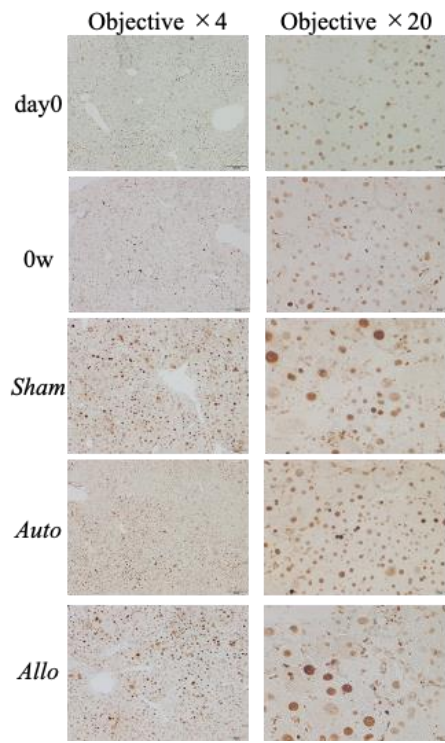


Figure5

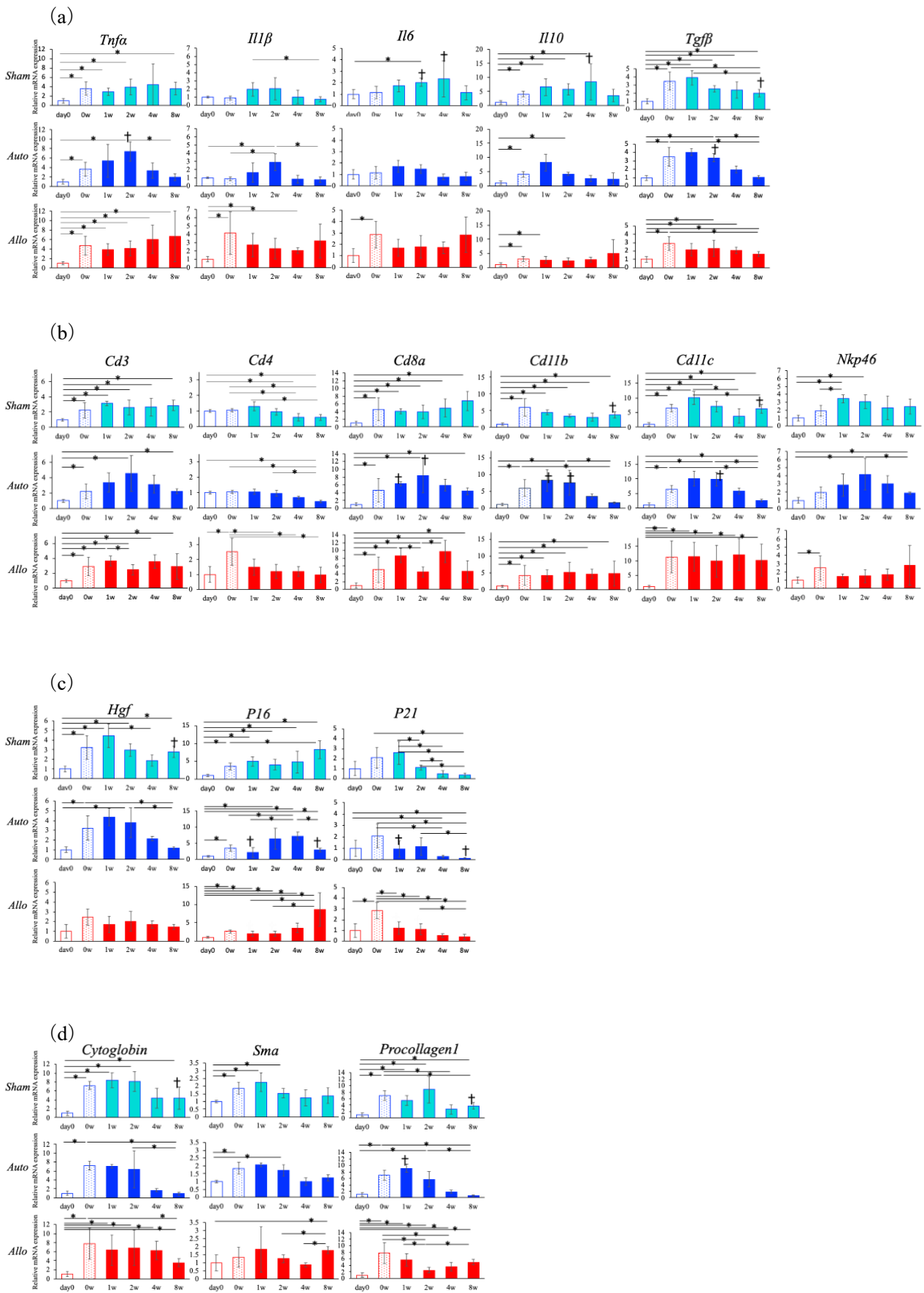
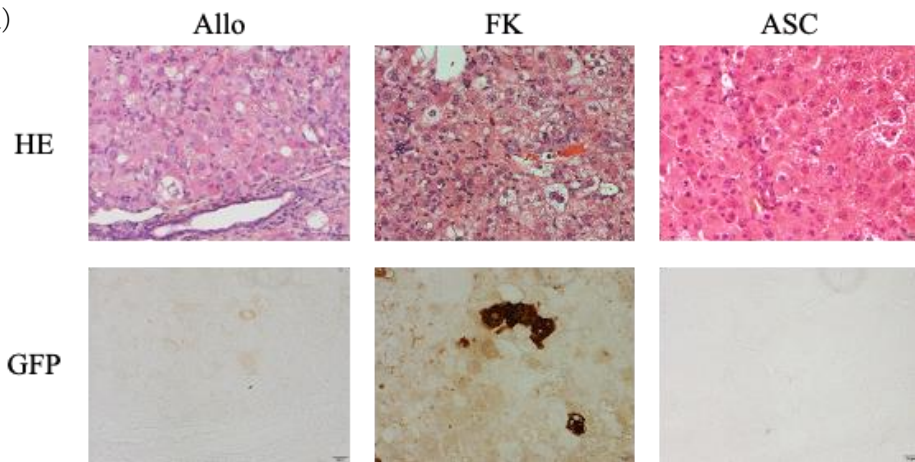
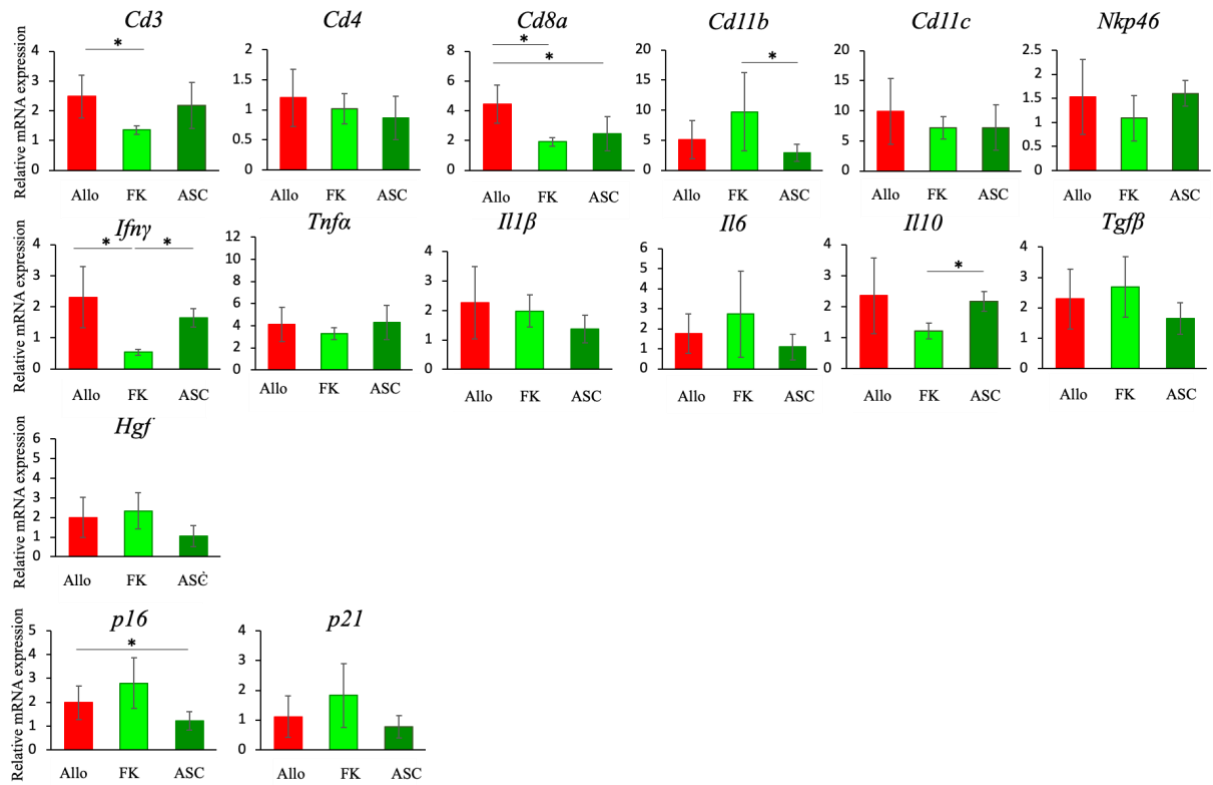


Figure6

(a)



(b)



Suppl. Fig. 1. Histology analysis of GFP immunostaining in Auto 8 weeks model.

- a. Histology of whole liver immunostained with GFP antibody (*Auto* model at 8 weeks after PH transplantation with RI of 54.7%). Scale bar: 200 μ l.
- b. Histological analysis with H&E staining at 8 weeks after PH transplantation in *Sham* (upper row), *Allo* (lower row). The area enclosed by lines indicate small hepatocytes. 4 \times objective's scale bar: 200 μ m, 20 \times objective's scale bar: 20 μ m.

Suppl. Fig. 2. Analysis of the sizes of the nuclei.

- a,b. The sizes of the nuclei in the liver sections with H&E staining were analyzed by using BZ-X800 and shown as histograms. The liver sections were observed at original magnification \times 20, and five random points were analyzed. The numbers indicate each median. a; Day 0 (left column) and 0 w (right column). b; *Sham* (upper row), *Auto* (middle row), and *Allo* (lower row) models. n = 3~5 in each group.

Suppl. Fig. 3. Hepatic mRNA expression in *Sham*, *Auto*, and *Allo* models.

Intrahepatic mRNA expression levels were measured by qRT-PCR. Expression levels of the respective mRNAs were normalized to that of GAPDH. In *Sham* and *Auto* model, the normalized data were presented as fold change compared with HSVtk/BL6 at day 0 for *Sham* and *Auto* models, and HSVtk/Balb at day 0 for *Allo* model (* p <0.05, † p <0.05 in comparison of the values between *Sham* and *Auto* models at the same time point). All the items were listed in the order of upper graph, that of *Sham*, *Auto* and *Allo* model. All the data are expressed as mean \pm SD. n = 3~5 in each group.

- a,b: The mRNA expressions of chemokines (a) and growth factors (b).

Suppl. Fig. 4. The influence and effect of the treatment against immune rejection.

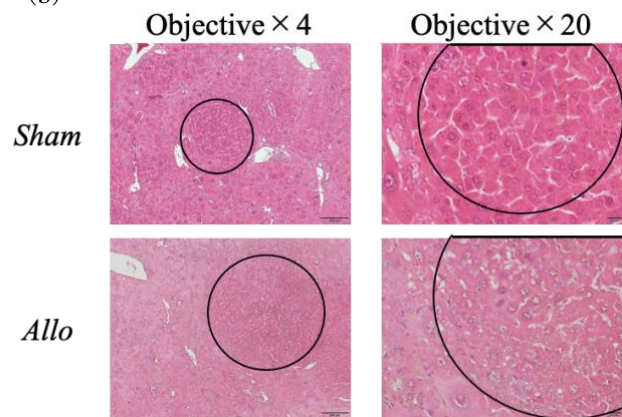
- a. Sequential changes of BW ratios in *Allo*, *FK*- and *ASC-treated* models. The Body weight ratio (the ratio of BW just before PH transplantation) was calculated for each week until 2 weeks after PH transplantation. n = 3~5 in each group.
- b. Sequential changes of ALT levels in *Allo*, *FK*- and *ASC-treated* models. ALT levels were measured every week from 0 to 2 weeks after PH transplantation. n = 3~5 in each group.
- c,d. Analysis of hepatocyte replacement rate in the treated models. GFP-positive areas of the tissue samples were calculated using ImageJ and average values (%) of hepatocyte replacement indices (RIs) were presented (c); hepatic mRNA expression levels of GFP mRNA were measured by qRT-PCR, expression levels of the mRNAs were normalized to that of GAPDH, and the values were presented as fold change compared with the those of *Auto* model at 1 week after transplantation (d). All the data are expressed as mean \pm SD. n = 3~5 in each group.

Suppl.Fig.1

(a)

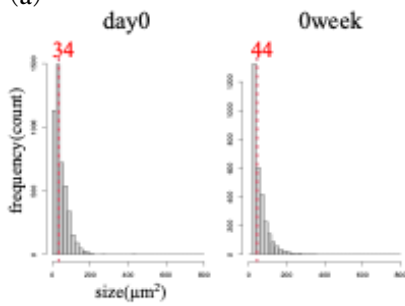


(b)

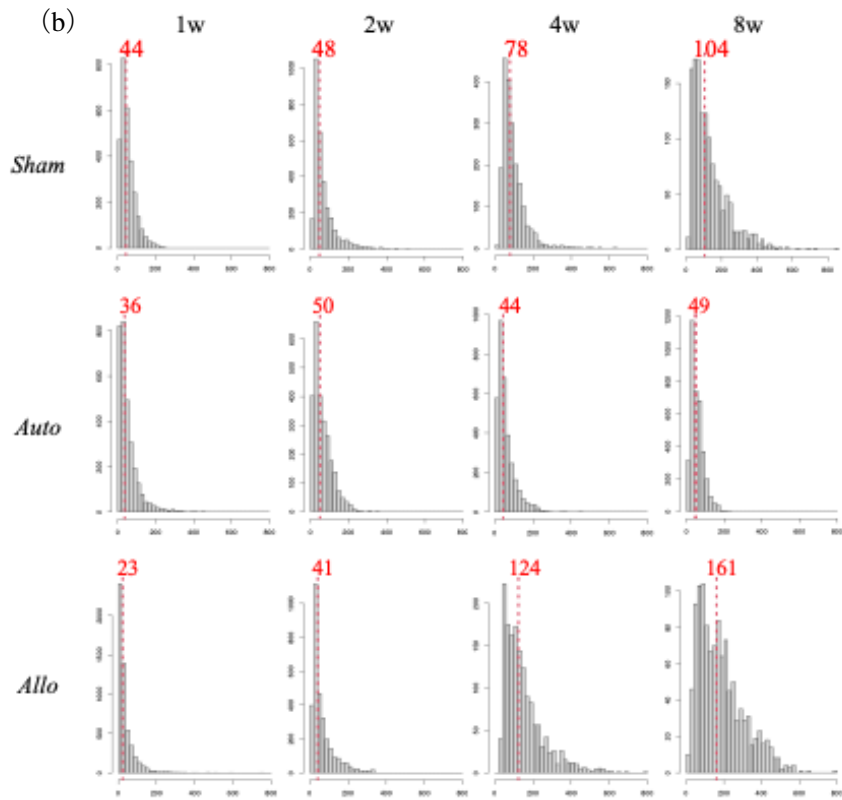


Suppl.Fig.2

(a)

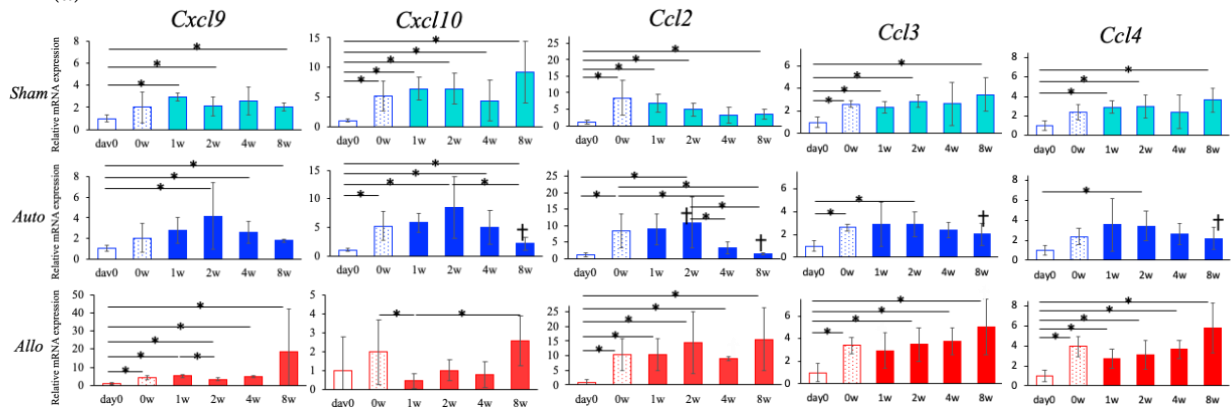


(b)

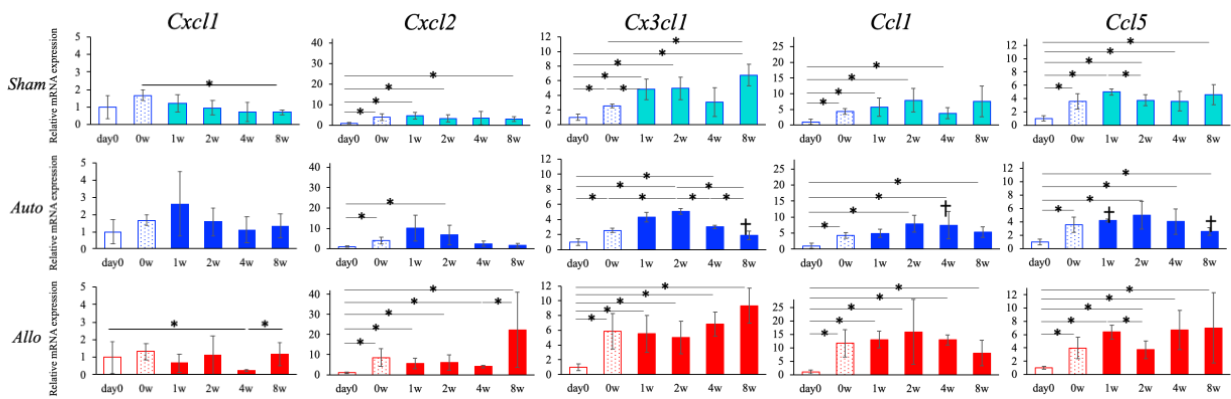


Suppl.Fig.3

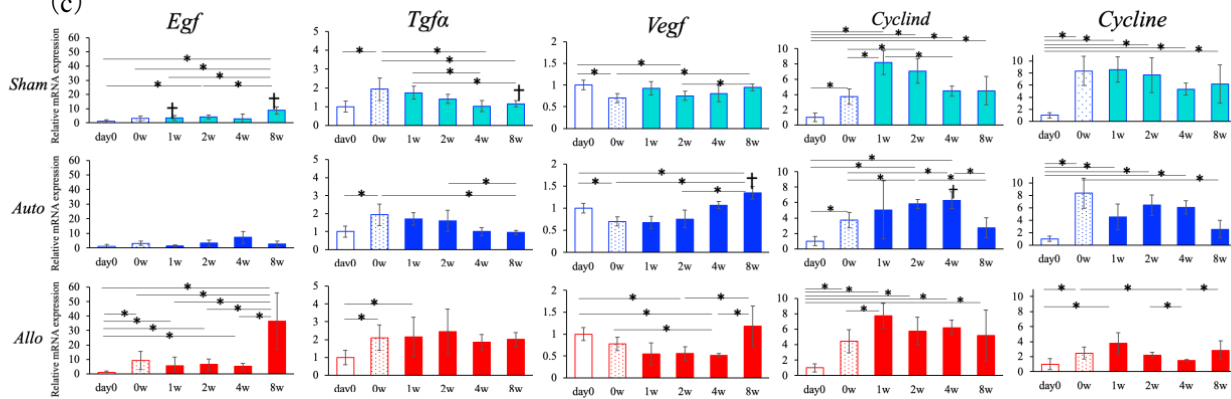
(a)



(b)

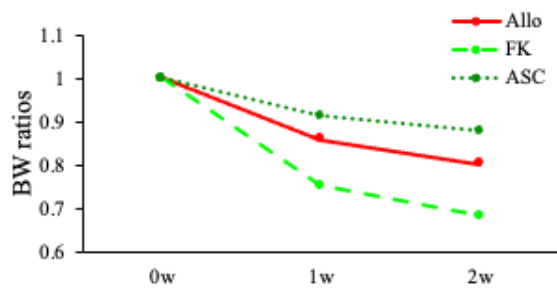


(c)

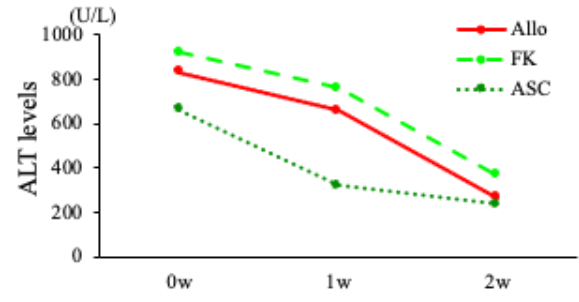


Suppl.Fig.4

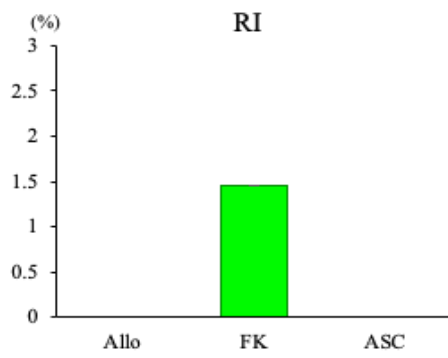
(a)



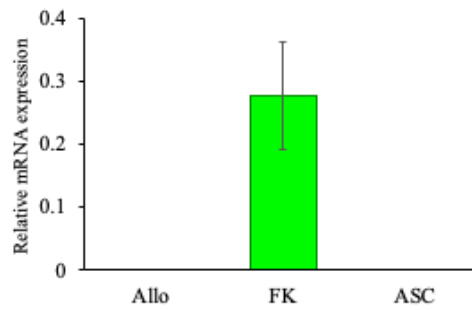
(b)



(c)



(d)



Suppl. Table 1. The combination of recipient and donor mice in each model.

	Recipient	Donor
<i>Sham</i>	HSVtk/BL6	—
<i>Auto</i>	HSVtk/BL6	GFPtg (BL6)
<i>Allo</i>	HSVtk/Balb	GFPtg (BL6)
<i>FK</i>	HSVtk/Balb	GFPtg (BL6)
<i>ASC</i>	HSVtk/Balb	GFPtg (BL6)

FK model (FK506-treated *Allo* model) and *ASC* model (ASC-treated *Allo* model) used the same recipient-donor combination as *Allo* model.

Suppl. Table 2. Primers used for qRT-PCR analysis in the study.

Gene	Forward primer sequences (5'--3')	Reverse primer sequences (5'--3')
<i>Ccl1</i>	CAGCAAGAGCATGCTTACGG	TTGAGGCGCAGCTTTCTCTA
<i>Ccl2</i>	GTGCTGAAGACCTTAGGGCAGA	AGCAGCAGGTGTCCCAAAGA
<i>Ccl3</i>	CATGACACTCTGCAACCAAGTCTTC	GAGCAAAGGCTGCTGGTTTCA
<i>Ccl4</i>	GGAGCTGCTCAGTTCAACTCCA	GAGACCAGCAGTCTTTGCTCCA
<i>Ccl5</i>	GGCTAGGACTAGAGCAAGCAATGAC	GGAGTATTTCTACACCAGCAGCAAG
<i>Cd3</i>	CTGGGCAACAATGCCAAAGA	AGCCGGATATGGTGCCTATGTTTA
<i>Cd4</i>	CAACCTGACTCTGACTCTGGACAA	AGGTAGGTCCCATCACCTCACA
<i>Cd8</i>	GTACTIONCAGTTCTGTCGTGCCAGTC	TCGCAGCACTGGCTTGGA
<i>Cd11b</i>	CCACTCATTGTGGGCAGCTC	GGGCAGCTTCATTCATCATGTC
<i>Cd11c</i>	AGGTCTGCTGCTGCTGGCTA	GGTCCCGTCTGAGACAAACTG
<i>Cd19</i>	CAACCAGTTGGCAGGATGATG	ATGACTGGGACCGGACTGAA
<i>Cdk2</i>	TCCGGATCTTTCGGACTCTG	ACAAGCTCCGTCCATCTTCA
<i>Cdk4</i>	CCAGGCAGGCTTTTCATTCA	AGGTCCTGGAAGTATGGGTG
<i>Cx3c1</i>	TCATGTGCGACAAGATGACC	GTGTCGTCTCCAGGACAATG
<i>Cxcl1</i>	CCGAAGTCATAGCCCACTCAA	GCAGTCTGTCTTCTTTCTCCGTTA
<i>Cxcl2</i>	GAAGTCATAGCCACTCTCAAGG	CCTCCTTTCCAGGTCAGTTAGC
<i>Cxcl9</i>	TTCCTGAGCAGTCCCAAATATCC	CTTCAGACATCTTCAGCGCACA
<i>Cxcl10</i>	TGTCCATCCATCGCAGCAC	ATCATCCCTGCGAGCCTATCC
<i>Cyclind</i>	GGGGACAACCTCTTAAGTCTCAC	CCAATAAAAGACCAATCTCTC
<i>Cyclind1</i>	AGGCGGATGAGAACAAGCAGA	CAGGCTTGACTCCAGAAGGG
<i>Cycline</i>	GAGCTTGAATACCCTAGGACTG	CGTCTCTCTGTGGAGCTTATAGAC
<i>Cytoglobin</i>	TCTGGAGGAGATCGCCGAGGAAT	CTTCTGCCCCAAAGTGCTGCCAG
<i>Egf</i>	AGCATACTCAGCGTCACAGC	GCAGGACCGGCACAAGTC
<i>Egfr</i>	CTGCCAAGGCACAAGTAACA	ATTGGGACAGCTTGGATCAC
<i>F4/80</i>	TCACTGTCTGCTCAACCGTC	TGCCATCAACTCATGATACCCT

<i>Gapdh</i>	TGTGTCCGTCGTGGATCTGA	TTGCTGTTGAAGTCGCAGGAG
<i>Gfp</i>	AACTCCAGCAGGACCATGTGAT	CACATGAAGCAGCAGCACTTCT
<i>Hgf</i>	GGCCCACTCATTTGTGAAC	CATCCACGACCAGGAAC
<i>Ifn-γ</i>	CGGCACAGTCATTGAAAGCCTA	GTTGCTGATGGCCTGATTGTC
<i>Il1 α</i>	TGGTTAAATGACCTGCAACAGGAA	AGGTCGGTCTCACTACCTGTGATG
<i>Il1β</i>	GAACGTCACACACCAGCAGGTTA	TCCAGGATGAGGACATGAGCAC
<i>Il6</i>	CCACTTCACAAGTCGGAGGCTTA	CCAGTTTGGTAGCATCCATCATTTC
<i>Il10</i>	GCCAGAGCCACATGCTCCTA	GATAAGGCTTGGCAACCCAAGTAA
<i>Ly6c</i>	TGCCTGCAACCTTGTCTGAG	GCTGGGCAGGAAGTCTCAAT
<i>Ly6g</i>	TTGCAAAGTCCTGTGTGCTC	GTCCAGAGTAGTGGGGCAGA
<i>Nkp46</i>	GACTAGGGCTCACAGAGGGACA	AAGAAGTAGGGTCGGTAGGTGC
<i>P16</i>	CGCAGGTTCTTGGTCACTGT	TGTTACGAAAGCCAGAGCG
<i>P21</i>	CCTGGTGATGTCCGACCTG	CCATGAGCGCATCGCAATC
<i>Procollagen1</i>	TGGTGCCAAGGGTGATACTG	CAATGGGACCAGTCAGACCA
<i>Sma</i>	TGGGTGACGAAGCACAGAGC	CTTCAGGGGCAACACGAAGC
<i>Tgfa</i>	CTCTGCTAGCGCTGGGTATC	TGGGCACTTGTGAAGTGAG
<i>Tgfβ</i>	GTGTGGAGCAACATGTGGAACCTA	CGCTGAATCGAAAGCCCTGTA
<i>Tnfa</i>	TATGGCCCAGACCCTCACA	GGAGTAGACAAGGTACAACCCATC
<i>Vegf</i>	CTGCTGTAACGATGAAGCCCTG	GCTGTAGGAAGCTCATCTCTCC
<i>Vegfr</i>	GGCGGTGGTGACAGTATCTT	TCTCCGGCAAGCTCAAT

Suppl. Table 3. Sequential changes of body weight (BW) ratios and ALT levels.

a. BW ratios

	0w	1w	2w	4w	8w
Sham	1.0±0.0	0.97±0.03	1.02±0.04	1.04±0.06	1.02±0.07
Auto	1.0±0.0	0.96±0.05	0.95±0.08	1.00±0.12	1.18±0.06
Allo	1.0±0.0	1.01±0.02	1.07±0.05	1.06±0.05	1.05±0.06
Treat- ment	FK	1.0±0.0	0.75±0.07	0.69±0.05	
	ASC	1.0±0.0	0.91±0.06	0.88±0.14	

b. ALT levels

	0w	1w	2w	4w	8w
Sham	494±119	208±58	321±21	268±135	425±175
Auto	456±98	160±61	192±41	216±127	82±61
Allo	869±439	246±105	344±209	402±136	507±211
Treat- ment	FK	918±111	760±300	365±53	
	ASC	660±167	319±27	237±107	